Published in final edited form as:
J Magn Reson Imaging. 2009 August ; 30(2): 366–373. doi:10.1002/jmri.21840.

Intraprocedural Diffusion-Weighted PROPELLER MRI to Guide Percutaneous Biopsy Needle Placement within Rabbit VX2 Liver Tumors

Jie Deng, PhD[1,2], **Sumeet Virmani, MD**[1], **Guang-Yu Yang, MD**[3], **Richard Tang**[1], **Gayle Woloschak, PhD**[4,5], **Reed A. Omary, MD**[1,2,5], and **Andrew C. Larson, PhD**[1,2,5]

[1]Department of Radiology, Northwestern University, Chicago, IL, USA

[2]Department of Biomedical Engineering, Northwestern University, Chicago, IL, USA

[3]Department of Pathology, Northwestern University, Chicago, IL, USA

[4]Department of Radiation Oncology, Northwestern University, Chicago, IL, USA

[5]Feinberg School of Medicine, Robert H. Lurie Comprehensive Cancer Center, Northwestern University, Chicago, IL, USA

Abstract

Purpose—To test the hypothesis that diffusion-weighted (DW)-PROPELLER (periodically rotated overlapping parallel lines with enhanced reconstruction) magnetic resonance imaging (MRI) can be used to guide biopsy needle placement during percutaneous interventional procedures to selectively target viable and necrotic tissues within VX2 rabbit liver tumors.

Materials and Methods—Our institutional Animal Care and Use Committee approved all experiments. In six rabbits implanted with 15 VX2 liver tumors, baseline DWPROPELLER images acquired prior to the interventional procedure were used for apparent diffusion coefficient (ADC) measurements. Next, intraprocedural DW-PROPELLER scans were performed with needle position iteratively adjusted to target viable, necrotic, or intermediate border tissue regions. DW-PROPELLER ADC measurements at the selected needle tip locations were compared with the percentage of tumor necrosis qualitatively assessed at histopathology.

Results—DW-PROPELLER images demonstrated intratumoral tissue heterogeneity and clearly depicted the needle tip position within viable and necrotic tumor tissues. Mean ADC measurements within the region-of-interest encompassing the needle tip were highly correlated with histopathologic tumor necrotic tissue assessments.

Conclusion—DW-PROPELLER is an effective method to selectively position the biopsy needle tip within viable and necrotic tumor tissues. The DW-PROPELLER method may offer an important complementary tool for functional guidance during MR-guided percutaneous procedures.

Keywords

diffusion-weighted imaging; PROPELLER; MRI guidance; percutaneous intervention; liver tumor

Please send correspondence and reprint requests to: Andrew C. Larson, Northwestern University, Department of Radiology, 737 N Michigan Ave, Suite 1600, Chicago, IL 60611, Tel: (312) 926-3499 Fax: (312)926-5991, a-larson@northwestern.edu.

INTRODUCTION

In the liver, percutaneous needle placement is currently used to 1) biopsy lesions for definitive diagnosis or 2) ablate tumors using thermal or chemical means. While ultrasound and computed tomography (CT) are the most commonly used needle guidance techniques, magnetic resonance imaging (MRI) is gaining increasing acceptance (1–10). MRI relies on susceptibility differences between the needle and background tissues. A recent study reported that MR-guided liver biopsies could be performed safely and accurately (3), providing diagnostic yields comparable to ultrasound- and CT-guided approaches (7).

Conventionally, MR-guided liver tumor biopsies have been performed using anatomic and/or contrast-enhanced (CE) images for intraprocedural navigation and sample targeting (1–6,8–10). However, these images may be inadequate to differentiate viable from necrotic tissues. Viable tissue is required for accurate histological confirmation of malignancy. Thus, the potential sampling errors that may result when using conventional anatomic guidance can 1) lead to insufficient material for diagnosis or 2) require additional tissue sampling, thereby increasing patient discomfort and bleeding risk. Furthermore, particularly for smaller hepatic lesions, rapid contrast wash-out times can lead to inadequate conspicuity of the target lesion (4) during needle placement.

Optimal positioning of interventional devices is critical during biopsy to reduce sampling error and during percutaneous ablation to treat the viable tumor regions. Previous studies have demonstrated that MR spectroscopy (11) and perfusion-weighted imaging (12–15) can provide complementary functional information to guide stereotactic biopsy in brain tumors. Diffusion weighted MRI (DWI) methods have been used to retrospectively correlate water mobility measurements with histopathologic characteristics at the biopsy sites (16–19).

DWI techniques employ tissue water mobility as an endogenous probe for noninvasive interrogation of microstructural tissue properties. Viable tumor tissues and tumor necrosis can be differentiated based on differences in local water mobility between these tissues (20–25). However, commonly used single-shot DW echo-planar imaging (EPI) techniques may be inappropriate for needle guidance during percutaneous procedures because the susceptibility-induced field inhomogeneities near interventional devices can lead to signal loss and severe geometric distortion.

Recently developed multishot PROPELLER (periodically rotated overlapping parallel lines with enhanced reconstruction) techniques (26) may improve image quality to facilitate accurate needle localizations for DWI-guided interventional procedures. PROPELLER is a turbo spin echo (TSE)-based technique, which acquires each data segment as a rotating rectilinear strip along a concentric propeller-shaped k-space trajectory. It is less sensitive to motion due to the oversampling of the central k-space region and averaging of low spatial frequency data. DW-PROPELLER methods have been used to quantify tumor necrotic fraction and viable tumor volume based on spatially resolved tumor viability maps (24) in a VX2 rabbit liver tumor model. Additionally, the TSE-based PROPELLER approaches are much less sensitive to local magnetic susceptibility variations that can lead to significant image distortions when using single-shot DW-EPI methods (27).

The purpose of our study was to determine the feasibility of using DW-PROPELLER methods to functionally guide percutaneous interventional procedures. We tested the hypothesis that intraprocedural DW-PROPELLER measurements can be used to selectively position biopsy needles within either viable or necrotic regions in VX2 rabbit liver tumors.

MATERIALS AND METHODS

Animal Model

All experiments were approved by our institutional Animal Care and Use Committee and were performed in accordance with institutional guidelines. Nine 4–5 kg New Zealand white rabbits were used for these experiments. VX2 cells were initially grown in the hindlimb of three donor rabbits. A small incision was made in the hepatic capsule of each rabbit and harvested tumor portions with 2 mm diameter were implanted during a mini-laparotomy procedure (28). In six rabbits a total of 15 VX2 liver tumors were implanted and allowed to grow for 3–4 weeks before imaging. VX2 rabbits provide a useful model for the biopsy needle targeting studies because as each VX2 tumor grows, necrotic regions are formed due to central hypoxic conditions within each tumor.

MR-Guided Percutaneous Procedures

All percutaneous procedures and imaging experiments were performed with rabbits positioned within a 1.5T clinical scanner (Magnetom Espree, Siemens Medical Solutions, Erlangen, Germany). Rabbits were imaged in the supine position using a four-channel head coil. Rabbits were intubated with a 3F endotracheal tube and administered isoflurane anesthesia using a small animal ventilator (Harvard Apparatus, Holliston, MA) throughout each imaging procedure (60–70 breaths/min).

Following initial localization, T2W-PROPELLER images were acquired at contiguous axial slice positions covering the entire liver volume with 3 mm slice thickness. Next, baseline DW-PROPELLER images were acquired at the same slice positions with the following parameters: field of view (FOV) = 200 × 200 mm^2, TR/TE = 3000/77 msec, matrix = 192 × 192, spatial resolution = 1.0 × 1.0 × 3.0mm^3, ETL = 21, number of blade = 60, BW = 789 Hz/pixel, b-value = 0, 534, and 866 s/mm^2. After baseline imaging, an MR-compatible clinical 22G aspiration biopsy needle (E-Z-EM, NY, USA) was inserted percutaneously into the selected rabbit liver tumor. The needle was inserted parallel to the axial imaging plane with insertion position, angle, and depth qualitatively estimated using the baseline T2W images. Next, serial T2W-PROPELLER and DWPROPELLER (b-value = 534 s/mm2) measurements were performed with needle position iteratively adjusted between measurements to target either viable, necrotic, or intermediate border tissue regions. During these iterative positioning procedures, we assumed that bright signal intensity within DW images and reduced water mobility within apparent diffusion coefficient (ADC) maps corresponded to viable tumor tissues. At final needle positions, for each selected tissue type, we repeated the acquisition of DW-PROPELLER images at b-value = 0, 534, and 866 s/mm2. For comparison purposes, we also acquired a set of single-shot DW-EPI images at the same slice positions using the following parameters: FOV = 200 × 110 mm^2, TR/TE = 3000/97 msec, matrix = 128 × 64, BW = 1500 Hz/pixel, average = 6, nonselective fat saturation, b-value = 0, 500, and 850 s/mm^2.

Following needle localization and imaging, the inner needle shaft was removed and a solution with 40–120 mm spherical polyvinyl alcohol (PVA) particles (blue color; Beadblock; Terumo Medical, Elkton, MD) was injected through the needle shell to permit gold-standard confirmation of needle tip position for histopathologic evaluation. Care was taken to maintain the needle position and depth within the tissue when injecting the bead solution.

For comparison purposes, prior to biopsy procedures we also acquired T1-weighted (T1W) gradient echo (GRE) images before and after intravenous gadopentetate-dimeglumine contrast injection (Magnevist; Berlex Laboratories, Wayne, NJ) at doses of 0.1 mmol/kg through a catheter in the rabbit's ear vein. Imaging parameters for T1W GRE were FOV = 220 ×124

mm2, TR/TE = 193/2 msec, flip angle = 80°, BW = 480 Hz/pixel, matrix = 256 × 144, average = 2.

Image Analysis

Image postprocessing was performed offline using MatLab software (MathWorks, Natick, MA). At each final needle tip position we selected a small region of interest (ROI) (10–15 mm^2) encompassing the needle tip within the DW-PROPELLER images. Each of these ROIs were transferred to the corresponding baseline DW-PROPELLER image series (without needle in place) and the ADC values within these ROIs were calculated using least squares fitting of DW signal intensities to a mono-exponential decay function. We also reconstructed full FOV ADC maps from each baseline DW image series.

Histopathologic Evaluation

Each rabbit was euthanized with commercial intravenous Beuthanasia solution containing pentobarbital (100 mg/kg). Rabbit livers were fixed in 10% buffered formaldehyde solution and sliced at 3–4 mm intervals in the axial plane to correspond to the plane of the MR images as closely as possible. For histopathologic examination we embedded in paraffin those tumor slices for which clusters of blue beads were observed. Tumors were sectioned into 4-μm slices and stained using hematoxylin and eosin (H&E) to differentiate viable tumor tissues and tumor necrosis. First, bead positions were located within the H&E slices to determine the needle tip location. Next, within regions surrounding these needle tip positions, H&E cell staining and cell morphology characteristics were used to qualitatively estimate the regional tissue necrotic fraction. These regions within the H&E slides were classified by an attending surgical pathologist with >10 years specialization experience in gastrointestinal oncology. Tumor necrosis was characterized as areas with completely hyalinized and necrotized tumor cell debris, whereas viable regions were characterized as pleomorphic and hypercellular tumor cells mostly in a solid and trabecular pattern. For display purposes, these H&E slides were digitized with optical magnification using a multispectral imaging system (Nuance, CRI, Woburn, MA) at both ×25 and ×100 magnifications. For inspection of complete tumor slices, ×25 magnified portions were stitched together using the PanaVue Image Assembler software (QC, Canada).

Statistical Analysis

For each final needle tip position, mean ADC within the ROI encompassing the needle tip was compared to reference standard histopathologic necrotic fraction measurements within the same areas. We calculated the linear correlation between these two sets of measurements using the linear regression model $Y = A + B * X$, where X was the histopathological necrotic fraction measurement, Y was the DW-PROPELLER ADC measurement, B the slope of the linear fitting line, and A the intercept. Additionally, the Pearson's correlation coefficient r was calculated with $P < 0.05$ considered statistically significant.

RESULTS

Percutaneous procedures were performed in six rabbits with a total of 15 VX2 liver tumors. These included two smaller (diameter = 1.65 ± 0.07 cm, mean ± SD) primarily viable tumors, one late-stage large tumor (diameter = 3.2 cm) with hemorrhage throughout, and 12 tumors (diameter = 2.1 ± 0.46 cm) containing a heterogeneous combination of necrotic and viable tissue types. For those VX2 tumors with intermediate size (diameter = 2.1 ± 0.46 cm), a necrotic central tissue core was typically surrounded by a viable periphery.

Representative examples of DW-PROPELLER images acquired with biopsy needle in place are shown in Figs. 1–3 along with corresponding ADC maps reconstructed from the baseline DW images. DW-PROPELLER images clearly depicted intratumoral tissue heterogeneity,

particularly for those larger VX2 tumors (diameter = 2.1 ± 0.46 cm), consisting of viable peripheral regions surrounding a central necrotic core. With increasing diffusion weighting, necrotic tumor cores demonstrated greater signal suppression than the peripheral viable tumor tissues. The resulting parametric ADC maps demonstrated central regions of higher ADC values relative to surrounding peripheral regions of lower ADC values. The MRI-compatible needles were clearly visualized in each DW image as signal voids along the needle track. Intratumoral tissue heterogeneity was better represented on DW images with higher b-value. CE-T1W images typically showed peripheral tumor enhancement corresponding to perfused, presumably viable regions of the VX2 tumors.

For the procedure depicted in Fig. 1, the needle tip was guided to a presumably viable region within the left-most tumor. For DW image at b = 0 s/mm^2 (Fig. 1a), signal within regions surrounding the needle tip were hypointense relative to hyperintense signal within central tumor core. For DW image at b = 866 s/mm^2 (Fig. 1c), signal within regions surrounding the needle tip was hyperintense relative to central tumor core and adjacent normal liver parenchyma. Within the baseline ADC map (Fig. 1d), mean ADC measured within an ROI at the final needle tip position (0.9×10^{-3} mm^2/s) was lower than mean ADC within the tumor core (2.3×10^{-3} mm^2/s). Digital images of the corresponding histopathology H&E slide (Fig. 1f–h) show a cluster of beads marking the needle tip position. Qualitatively, the needle tip position depicted within the intraprocedural DW images correlated to the bead position within the H&E images (Fig. 1f). These beads were located within a tissue region characterized as 95% viable (Fig. 1h).

For the procedure depicted in Fig. 2, the needle tip was guided to an intermediate region at the interface between presumably viable periphery and central necrotic core. Within the baseline ADC map (Fig. 2d), mean ADC measured within an ROI at the needle tip position (1.7×10^{-3} mm^2/s) was lower than mean ADC within the tumor core (2.5×10^{-3} mm^2/s) but higher than mean ADC within the viable periphery (0.5×10^{-3} mm^2/s). Digital images of the corresponding histopathology H&E slide (Fig. 2f–h) show a cluster of beads marking the needle tip position. These beads were located within a tissue region characterized as 50% viable and 50% necrotic tissues (Fig. 2h).

For the procedure depicted in Fig. 3, the needle tip was guided to a small presumably necrotic region located at the tumor periphery within the upper tumor. For DW image at b = 0 s/mm^2 (Fig. 3a), signal within the region surrounding the needle tip was hyperintense relative to hypointense signal within peripheral viable regions. For DW image at b = 866 s/mm^2 (Fig. 3c), signal within regions surrounding the needle tip were hypointense relative to surrounding viable tissues. Within the baseline ADC map (Fig. 3d), mean ADC measured within an ROI at the needle tip position (2.2×10^{-3} mm^2/s) was higher than mean ADC within the viable tumor periphery (0.71×10^{-3} mm^2/s). Digital images of the corresponding histopathology H&E slide (Fig. 3f–h) show a cluster of beads marking the needle tip position. These beads were located within a tissue region characterized as 95% tumor necrosis (Fig. 3h).

DW-PROPELLER images (b = 866 s/mm^2) collected during separate procedures in six additional animals are shown in Fig. 4. Overall, viable tumor tissues demonstrated higher signal intensity compared to necrotic tissues within the central tumor cores on these high b-value DW images. During the procedure depicted in Fig. 4a, the needle was inserted into a tumor area with homogeneous intratumoral DW signal intensity, hyperintense relative to adjacent normal liver tissues. For this example, tissues surrounding the needle tip position were later classified as 90% viable at histopathology. During the procedure depicted in Fig. 4b, the needle was positioned between two adjacent tumors with the tip located within the outer viable region of the left-most tumor. During procedures depicted in Fig. 4c,e, the biopsy needle tip was positioned within intermediate regions at the interface between suspected viable periphery and

necrotic tissue core. These intermediate regions were later classified at histopathology as a mixed tissue type containing 50% viable and 50% necrotic tissues. During procedures depicted in Fig. 4f,g, the biopsy needle tip was positioned within hypointense regions relative to hyperintense peripheral regions. For these two examples, tissues surrounding the needle tip positions were later classified as >90% tumor necrosis at histopathology.

Additionally, two representative single-shot DW-EPI images ($b = 850$ s/mm^2), acquired at the same slice positions as DW-PROPELLER images (Fig. 4b,g), are shown in Fig. 4d,h, respectively. Within the DW-EPI images, severe image distortion and chemical shift artifacts obscured the description of both hepatic and tumor anatomy adjacent to the needle positions. Stron field inhomogeneities induced by the needle also increased the perceived needle width and interfered with needle tip localization. Compared with the DW-EPI images, qualitatively, the shape and size of the needle artifacts (ie, signal voids) were much smaller in the DW-PROPELLER images, which could potentially permit improved precision during needle tip localization.

At a total of 23 needle positions within 15 VX2 tumors, mean ADC values within the ROIs encompassing the needle tips were compared with the percentage of tumor necrosis qualitatively assessed at histopathology (Fig. 5). DW-PROPELLER ADC measurements were highly correlated with histopathologic necrotic fraction measurements ($Y = 0.63 + 0.019 * X$; $r = 0.926$, $P < 0.0001$). In six tumor regions with 80%–100% viable tumor tissues surrounding the needle tips, ADC values were $0.88 \pm 0.28 \times 10^{-3}$ mm^2/s (mean ± SD), indicating highly restricted water diffusion within the well-organized and high cell density viable tumor tissues. In seven tumor regions with heterogeneous distributions of viable tissues and tumor necrosis, ADC values were $1.45 \pm 0.23 \times 10^{-3}$ mm^2/s (mean ± SD), indicting increasing water mobility within these intermediate damaged tissues. In 10 tumor regions with 90%–100% necrosis, ADC values were $2.51 \pm 0.36 \times 10^{-3}$ mm^2/s (mean ± SD), which could be attributed to compromised cell membranes, regions of liquefied tumor necrosis, and complete tumor hemorrhage, each permitting greater diffusion of water molecules within these necrotic tissue regions.

DISCUSSION

In this preclinical study, we tested the feasibility of using multishot DW-PROPELLER MRI to provide functional guidance during needle placement within rabbit VX2 liver tumors. DW-PROPELLER images permitted selective positioning of the biopsy needle tip within viable and necrotic tissues. Baseline DW-PROPELLER ADC measurements at the selected needle tip locations were strongly correlated with histologic assessments of tumor tissue necrosis. Within conventional single-shot DW-EPI images, tissues adjacent to the biopsy needle were severely distorted, precluding precise intraprocedural localization. A variety of sequences have previously been employed for MR-guided percutaneous interventions including balanced steady-state free precession sequence (eg, TrueFISP (29)), fast low angle shot (FLASH) (8, 30), and TSE sequences (31,32). However, conventional T2- or T1-weighted image contrast may not distinguish viable from necrotic tumor regions. Inadequate targeting of viable tumor tissue may result in sampling errors during biopsy procedures and reduced therapeutic efficacy during percutaneous interventional therapies. These shortcomings have motivated clinicians to incorporate functional imaging methods to optimize target selection. Previous studies have demonstrated the efficacy of multispectral segmentation methods based on proton density, T1- and T2-weighted images for classification of tissue types within brain tumors, later confirmed via histopathology following stereotactic biopsy (33). Perfusion-weighted MRI measurements providing cerebral blood volume (CBV) and flow (CBF) maps have been used for preoperative assessment of tumor grade and localization of active, expanding tumor regions targeted for stereotactic biopsy (12,13,15). More recently, tissue water mobility measurements using DWI

techniques in brain tumors were retrospectively correlated with histopathology findings at the identical biopsy sites (16–19), suggesting the potential to use DWI to facilitate stereotactic surgical planning.

Use of conventional single-shot DW-EPI techniques may be challenging during percutaneous interventional procedures, particularly within the abdomen. Precise coregistration of baseline DW-EPI images with anatomic guidance images acquired during percutaneous procedures could be difficult due to the commonly severe distortion and image artifacts. Furthermore, acquisition of intraprocedural DW-EPI images (with percutaneous device in place) may simply be inappropriate because these devices lead to even further, often severe, geometric distortion as demonstrated in preclinical VX2 animal model studies (24). Multishot TSE-based DWPROPELLER is less sensitive to susceptibility-induced field gradients near the interventional device, allowing improved depiction of the needle and more precise localization during functional targeting of viable and necrotic tissues. DW-PROPELLER also offers the potential for increased spatial resolution. As shown in previous VX2 tumor studies (24), DW-PROPELLER images and resultant parametric ADC measurements can generate spatially resolved intratumoral viability maps strongly correlated with histopathology. Given these salient features, DW-PROPELLER may be an accurate technique to guide placement of either biopsy or ablation needles into viable, functionally active portions of targeted tumors.

Contrast-enhanced MRI can improve lesion conspicuity and thus facilitate stereotactic MRI-guided interventions (1,2,5,6,9). Within CE images, enhancing regions are typically considered viable. During the current VX2 studies, CE-T1W images qualitatively demonstrated less intratumoral heterogeneity than corresponding DW images and reduced enhancing area compared to restricted diffusion, high-signal intensity area within corresponding DW images. Further systematic studies are necessary to rigorously compare CEMRI and DWI techniques to determine the functional origin of these discrepancies. However, for needle guidance, CE methods are inherently limited by contrast dose limitations and variable transit times within the targeted tissues. Rapid contrast wash-out times within a targeted lesion could complicate accurate targeting, particularly for extended procedure durations (4). DWI uses local water mobility as an endogenous probe for noninvasive interrogation of tissue microstructure, and therefore DWI measurements can be repeatedly performed throughout an interventional procedure. Further studies are necessary to compare CE-MRI and DWI techniques as complementary imaging tools for functional targeting during MR-guided interventions.

The direct benefit of DW-PROPELLER as pertains to liver tumor biopsy in the clinical setting requires further investigation. In the VX2 rabbit study (24) DW imaging methods have been particularly effective for differentiating viable and necrotic tumor tissues; however, alternative methods could certainly be used to visualize hemorrhage (T2*-weighted measurements) and tumor involvement in the liver (STIR, T1-weighted, and T2-weighted measurements). Further studies are warranted to fully investigate the complementary benefits of these anatomic MRI methods and proposed functional DW-PROPELLER approaches in the setting of liver tumor biopsy.

There were several important limitations to this study. First, in this feasibility study we chose to inject PVA particles to confirm positioning with pathology rather than directly collect tissue samples from the biopsy needles. Our rationale was that the harvested tissue specimens, especially from necrotic regions, would be more likely to be disrupted during core needle biopsy and thus more difficult to spatially correlate with imaging. With aspiration biopsy cytology, the microscopic examination of single cell architecture may inadequately correlate with the regions of tumor deemed viable with noninvasive imaging. However, based on the success of this study, we plan to undertake a future study that aims to correlate tissue specimens obtained under this functional MRI guidance system with the imaging features of sampled

tissue. Second, the long acquisition time for DW-PROPELLER images (3 minutes for each stack of DW images at one b-value) precludes real-time use of this guidance method. Similar to most CT-guided needle placement techniques, needle position in this study was identified after advancement of the needle. For future clinical settings, we propose that an alternative MRI sequence (such as gradient echo and single-shot TSE) be used to position the needle in real time, and then DW-PROPELLER be added to confirm final location in a functionally active portion of the tumor prior to sampling. Finally, additional technical development of DW-PROPELLER methods will be necessary to reduce acquisition time. Several approaches that could be incorporated to reduce acquisition time include k-space undersampling (35), parallel imaging (34), and inner volume imaging (32,36). Such approaches may be critical to accelerate DW-PROPELLER scan time for more practical clinical applications. Prior to clinical translation, we recommend that additional animal studies be performed using these techniques to verify improved diagnosis accuracy.

In conclusion, we have demonstrated the feasibility of using DW-PROPELLER MRI to guide biopsy needle placement to selectively target viable tissues within VX2 rabbit liver tumors. DW-PROPELLER is a promising method to optimize placement of percutaneous devices during interventional procedures. Future translational studies should evaluate the use of the DWPROPELLER techniques for functional targeting during MR-guided percutaneous procedures in liver cancer patients.

Acknowledgments

This research is supported by funds from: NIH NCI R01CA134719.

REFERENCES

1. Daniel BL, Birdwell RL, Butts K, et al. Freehand iMRI-guided largegauge core needle biopsy: a new minimally invasive technique for diagnosis of enhancing breast lesions. J Magn Reson Imaging 2001;13:896–902. 372 Deng et al. [PubMed: 11382950]
2. Helbich TH. Localization and biopsy of breast lesions by magnetic resonance imaging guidance. J Magn Reson Imaging 2001;13:903–911. [PubMed: 11382951]
3. Kariniemi J, Blanco Sequeiros R, Ojala R, Tervonen O. MRI-guided abdominal biopsy in a 0.23-T open-configuration MRI system. Eur Radiol 2005;15:1256–1262. [PubMed: 15627187]
4. Konig CW, Trubenbach J, Fritz J, Lauer UM, Claussen CD, Pereira PL. Contrast enhanced MR-guided biopsy of hepatocellular carcinoma. Abdom Imaging 2004;29:71–76. [PubMed: 15160756]
5. Obenauer S, Grabbe E, Knollmann F. Value of MR-guided localization and biopsy in breast lesions. Rofo 2006;178:477–483. [PubMed: 16708322]
6. Parkkola RK, Mattila KT, Heikkila JT, et al. Dynamic contrastenhanced MR imaging and MR-guided bone biopsy on a 0.23 T open imager. Skeletal Radiol 2001;30:620–624. [PubMed: 11810153]
7. Schmidt AJ, Kee ST, Sze DY, et al. Diagnostic yield of MR-guided liver biopsies compared with CT- and US-guided liver biopsies. J Vasc Interv Radiol 1999;10:1323–1329. [PubMed: 10584646]
8. Silverman SG, Collick BD, Figueira MR, et al. Interactive MR guided biopsy in an open-configuration MR imaging system. Radiology 1995;197:175–181. [PubMed: 7568819]
9. Viehweg P, Heinig A, Amaya B, Alberich T, Laniado M, Heywang-Kobrunner SH. MR-guided interventional breast procedures considering vacuum biopsy in particular. Eur J Radiol 2002;42:32–39. [PubMed: 12039018]
10. Zimmermann H, Muller S, Gutmann B, et al. Targeted-HASTE imaging with automated device tracking for MR-guided needle interventions in closed-bore MR systems. Magn Reson Med 2006;56:481–488. [PubMed: 16795081]
11. De Edelenyi FS, Rubin C, Esteve F, et al. A new approach for analyzing proton magnetic resonance spectroscopic images of brain tumors: nosologic images. Nat Med 2000;6:1287–1289. [PubMed: 11062544]

12. Chaskis C, Stadnik T, Michotte A, Van Rompaey K, D'Haens J. Prognostic value of perfusion-weighted imaging in brain glioma: a prospective study. Acta Neurochir (Wien) 2006;148:277–285. discussion 285. [PubMed: 16421765]
13. Maia AC Jr, Malheiros SM, da Rocha AJ, et al. Stereotactic biopsy guidance in adults with supratentorial nonenhancing gliomas: role of perfusion-weighted magnetic resonance imaging. J Neurosurg 2004;101:970–976. [PubMed: 15597757]
14. Jun P, Garcia J, Tihan T, McDermott MW, Cha S. Perfusion MR imaging of an intracranial collision tumor confirmed by image guided biopsy. AJNR Am J Neuroradiol 2006;27:94–97. [PubMed: 16418364]
15. Weber MA, Risse F, Giesel FL, Schad LR, Kauczor HU, Essig M. Perfusion measurement using the T2* contrast media dynamics in neuro-oncology. Physical basics and clinical applications. Radiologe 2005;45:618–632. [PubMed: 15098092]
16. Beppu T, Inoue T, Shibata Y, et al. Measurement of fractional anisotropy using diffusion tensor MRI in supratentorial astrocytic tumors. J Neurooncol 2003;63:109–116. [PubMed: 12825815]
17. Leuthardt EC, Wippold FJ 2nd, Oswood MC, Rich KM. Diffusion weighted MR imaging in the preoperative assessment of brain abscesses. Surg Neurol 2002;58:395–402. discussion 402. [PubMed: 12517619]
18. Stadlbauer A, Ganslandt O, Buslei R, et al. Gliomas: histopathologic evaluation of changes in directionality and magnitude of water diffusion at diffusion-tensor MR imaging. Radiology 2006;240:803–810. [PubMed: 16926329]
19. Sugahara T, Korogi Y, Kochi M, et al. Usefulness of diffusion weighted MRI with echo-planar technique in the evaluation of cellularity in gliomas. J Magn Reson Imaging 1999;9:53–60. [PubMed: 10030650]
20. Geschwind JF, Artemov D, Abraham S, et al. Chemoembolization of liver tumor in a rabbit model: assessment of tumor cell death with diffusion-weighted MR imaging and histologic analysis. J Vasc Interv Radiol 2000;11:1245–1255. [PubMed: 11099235]
21. Chan JH, Tsui EY, Luk SH, et al. Diffusion-weighted MR imaging of the liver: distinguishing hepatic abscess from cystic or necrotic tumor. Abdom Imaging 2001;26:161–165. [PubMed: 11178693]
22. Kamel IR, Bluemke DA, Ramsey D, et al. Role of diffusion-weighted imaging in estimating tumor necrosis after chemoembolization of hepatocellular carcinoma. AJR Am J Roentgenol 2003;181:708–710. [PubMed: 12933464]
23. Deng J, Rhee TK, Sato KT, et al. In vivo diffusion-weighted imaging of liver tumor necrosis in the VX2 rabbit model at 1.5 Tesla. Invest Radiol 2006;41:410–414. [PubMed: 16523024]
24. Deng J, Virmani S, Young J, et al. Diffusion-weighted PROPELLER MRI for quantitative assessment of liver tumor necrotic fraction and viable tumor volume in VX2 rabbits. J Magn Reson Imaging 2008;27:1069–1076. [PubMed: 18407540]
25. Yuan YH, Xiao EH, Liu JB, et al. Characteristics of liver on magnetic resonance diffusion-weighted imaging: dynamic and image pathological investigation in rabbit liver VX-2 tumor model. World J Gastroenterol 2008;14:3997–4004. [PubMed: 18609683]
26. Pipe JG. Motion correction with PROPELLER MRI: application to head motion and free-breathing cardiac imaging. Magn Reson Med 1999;42:963–969. [PubMed: 10542356]
27. Forbes KP, Pipe JG, Karis JP, Heiserman JE. Improved image quality and detection of acute cerebral infarction with PROPELLER diffusion-weighted MR imaging. Radiology 2002;225:551–555. [PubMed: 12409594]
28. Virmani S, Harris KR, Szolc-Kowalska B, et al. Comparison of two different methods for inoculating VX2 tumors in rabbit livers and hind limbs. J Vasc Interv Radiol 2008;19:931–936. [PubMed: 18503910]
29. Duerk JL, Lewin JS, Wendt M, Petersilge C. Remember true FISP? A high SNR, near 1-second imaging method for T2-like contrast in interventional MRI at .2 T. J Magn Reson Imaging 1998;8:203–208. [PubMed: 9500281]
30. Puls R, Stroszczynski C, Rosenberg C, et al. Three-dimensional gradient-echo imaging for percutaneous MR-guided laser therapy of liver metastasis. J Magn Reson Imaging 2007;25:1174–1178. [PubMed: 17520737]

31. Butts K, Pauly JM, Daniel BL, Kee S, Norbash AM. Management of biopsy needle artifacts: techniques for RF-refocused MRI. J Magn Reson Imaging 1999;9:586–595. [PubMed: 10232519]

32. Buecker A, Adam G, Neuerburg JM, Glowinski A, van Vaals JJ, Guenther RW. MR-guided biopsy using a T2-weighted single-shot zoom imaging sequence (Local Look technique). J Magn Reson Imaging 1998;8:955–959. [PubMed: 9702898]

33. Vinitski S, Gonzalez C, Andrews D, et al. In vivo validation of tissue segmentation based on a 3D feature map using both a hamster brain tumor model and stereotactically guided biopsy of brain tumors in man. J Magn Reson Imaging 1998;8:814–819. [PubMed: 9702882]

34. Skare, S.; Newbould, R.; Bammer, R. Continuous 2D GRAPPA kernel for propeller trajectories. Proc 15th Annual Meeting ISMRM; Berlin. 2007. p. 1743

35. Arfanakis K, Tamhane AA, Pipe JG, Anastasio MA. k-Space undersampling in PROPELLER imaging. Magn Reson Med 2005;53:675–683. [PubMed: 15723398]

36. Feinberg DA, Hoenninger JC, Crooks LE, Kaufman L, Watts JC, Arakawa M. Inner volume MR imaging: technical concepts and their application. Radiology 1985;156:743–747. [PubMed: 4023236]

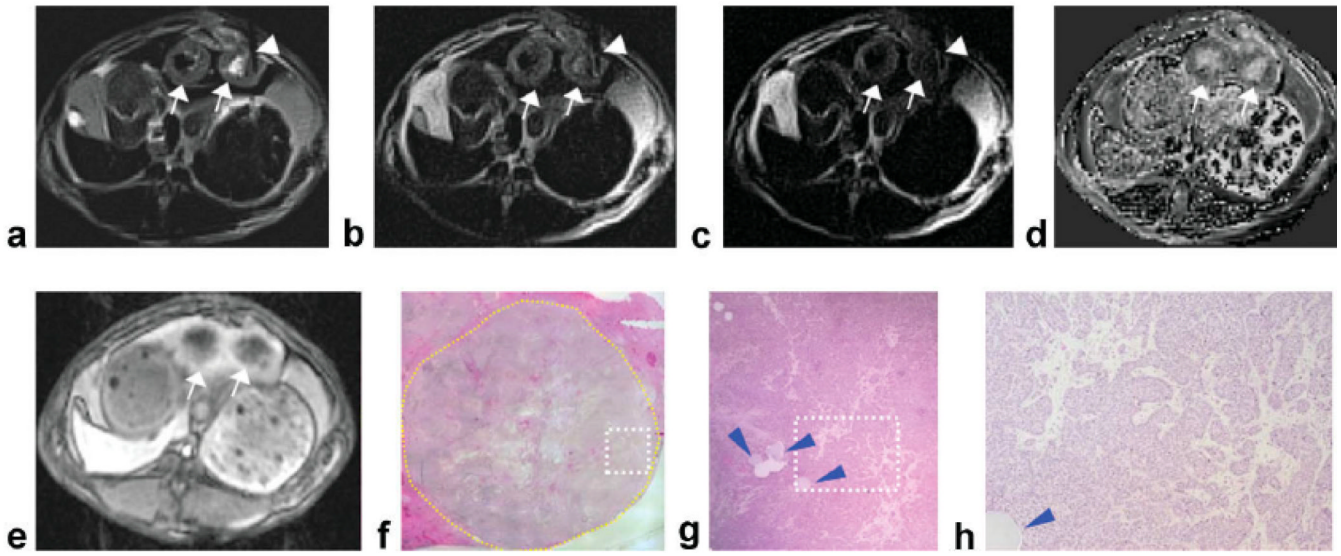

Figure 1.

Two adjacent VX2 rabbit liver tumors (arrows) with central tumor necrotic core and viable tumor periphery. DW-PROPELLER images (a–c) were acquired with needle (arrowheads) positioned to target the viable region of the left-most tumor (diameter = 1.6 cm). The corresponding ADC map reconstructed from baseline DW images demonstrated decreased water mobility at the position of needle placement (d). Contrast-enhanced T1W images at the arterial phase demonstrated perfusion of the tumor periphery (e). Overview H&E pathology image (×25 magnification) (f) of the left-most tumor (yellow contour line at tumor border) shows central necrotic core with viable tumor periphery. Magnified image (g) from inset within ×25 overview image (white dashed-box) shows the location of the injected beads (blue arrowheads) that served as our ex vivo reference for needle tip position. Tumor tissues within the region of bead deposition (×100 magnification image h from inset position within g) were classified as 95% viable at histopathology. Note: Signal void within the center of the right tumor in DW images was due to percutaneous injection of an iron-oxide agent during a previous imaging procedure.

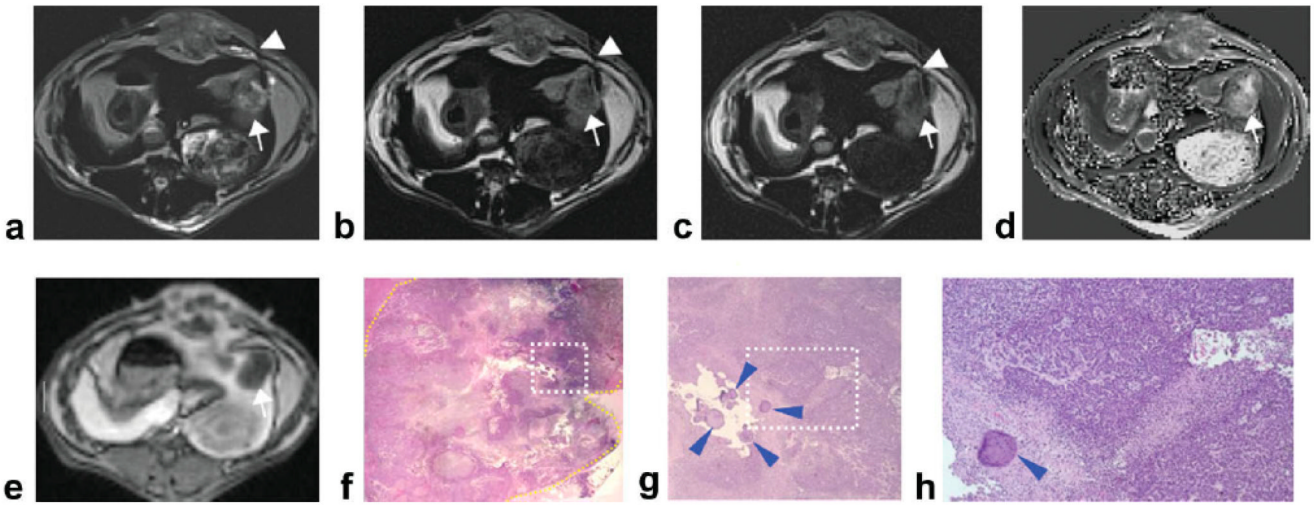

Figure 2.
Left lobe VX2 rabbit liver tumor (diameter = 2.2 cm) (arrows) with intratumoral heterogeneous distribution of viable and necrotic tumor tissues. DW-PROPELLER images (a–c) were acquired with needle (arrowheads) positioned to target the intermediate region at the interface between viable periphery and central necrotic core. Corresponding baseline ADC map shown at right (d). Contrast-enhanced T1W images demonstrate perfusion of the tumor periphery (e). Overview H&E pathology image (×25 magnification) (f) of the tumor (yellow contour line at lesion border) shows central necrotic core with viable tumor periphery and also heterogeneous distribution of mixed tissue types. Magnified image (g) from inset within ×25 overview image (white dashed-box in f) shows the location of the injected beads (blue arrowheads) which served as our ex vivo reference for needle tip position. Tumor tissues within the region of bead deposition (×100 magnification image h from inset position within g) were classified as 50% viable at histopathology.

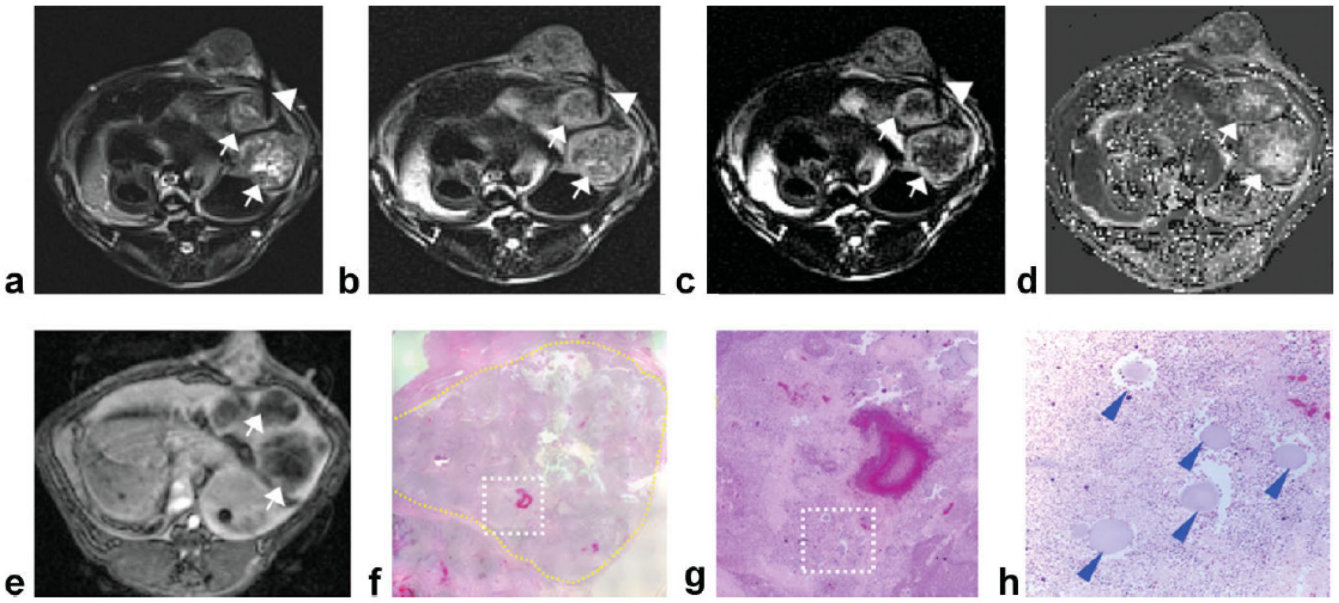

Figure 3.

Two adjacent VX2 rabbit liver tumors (arrows) with central tumor necrotic core and viable tumor periphery. DWPROPELLER images (a–c) were acquired with needle (arrowheads) positioned to target a small necrotic region located within the tumor periphery of the upper tumor (diameter = 1.7 cm). The corresponding ADC map reconstructed from baseline DW images demonstrated increased ADC measurements at the position of needle placement compared to surrounding viable tissues (d). Contrast-enhanced T1W images demonstrate perfusion of the tumor periphery (e). Overview H&E pathology image (×25 magnification) (**f**) of the upper tumor (yellow contour line at tumor border) shows intratumoral heterogeneous distribution of viable and necrotic tumor tissues. Magnified image (g) from inset within ×25 overview image (white dashed-box) shows the location of the injected beads (blue arrowheads) which served as our ex vivo reference for needle tip position. Tumor tissues within the region of bead deposition (×100 magnification image h from inset position within g) were classified as 100% necrotic at histopathology.

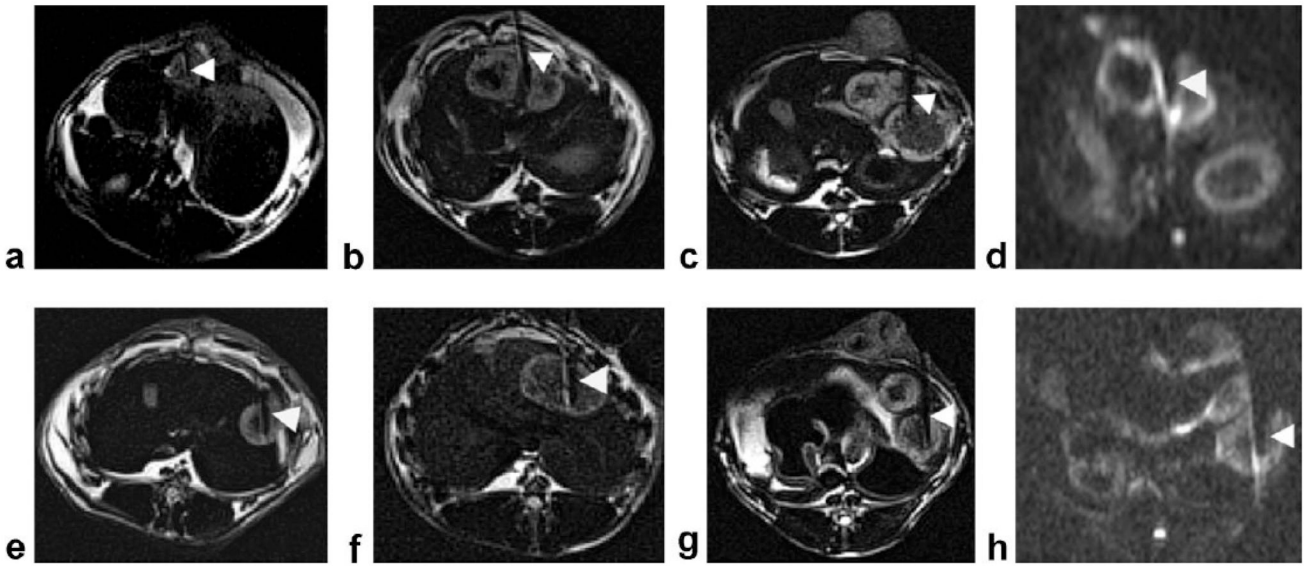

Figure 4.

DW-PROPELLER images (b = 866 s/mm^2) (a–c,e–g) acquired with needle (arrowheads) in six additional animals. For procedure (a) the needle was inserted into a small tumor with homogeneous hyperintensity relative to liver parenchyma and tumor tissues around the needle tip positions were characterized as 90% viable at histopathology. For procedure (b) the needle was positioned between two adjacent tumors with the tip located within the hyperintense outer region of the left-most tumor; tumor tissues around the needle tip position were characterized as 80% viable. For procedures (c,e) the biopsy needle tip was positioned within an intermediate region at the interface between viable periphery and necrotic tissue core; tissues in this region were later characterized as 50% viable. For procedures (f,g) the needle tip was positioned within tissues characterized as 100% necrotic at histopathology. Severe image distortion within two representative single-shot DW-EPI images (b = 850 s/mm^2) (d,h), acquired at the same slice positions as DW-PROPELLER images (b,g), obscures depiction of hepatic and tumor anatomy adjacent to needle positions.

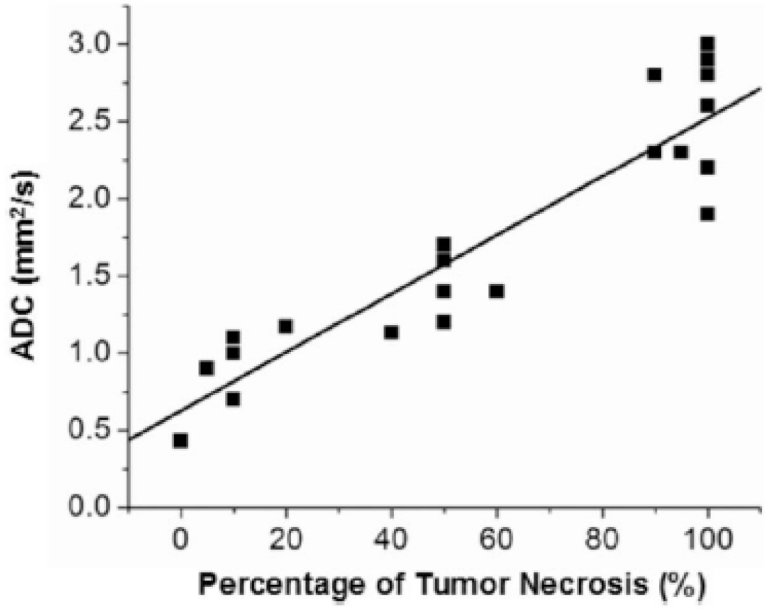

Figure 5.
Correlation of DW-PROPELLER ADC measurements, within an ROI surrounding biopsy needle tips, to corresponding reference standard histology measurements at 23 needle positions within 15 VX2 rabbit liver tumors.